Effects of temperature on the rupture strength and elastic stiffness of geogrids

W. Kongkitkul[1], W. Tabsombut[2], C. Jaturapitakkul[3] and F. Tatsuoka[4]

[1]*Assistant Professor, Department of Civil Engineering, King Mongkut's University of Technology Thonburi, 126 Pracha Uthit Rd., Bang Mod, Thung Khru, Bangkok 10140, Thailand, Telephone: +66 2 470 9144, Telefax: +66 2 427 9063, E-mail: warat.kon@kmutt.ac.th*
[2]*Formerly Graduate Student, Department of Civil Engineering, King Mongkut's University of Technology Thonburi, 126 Pracha Uthit Rd., Bang Mod, Thung Khru, Bangkok 10140, Thailand, Telephone: +66 2 470 9155, Telefax: +66 2 427 9063, E-mail: nae47210950@hotmail.com*
[3]*Professor, Department of Civil Engineering, King Mongkut's University of Technology Thonburi, 126 Pracha Uthit Rd., Bang Mod, Thung Khru, Bangkok 10140, Thailand, Telephone: +66 2 470 9137, Telefax: +66 2 427 9063, E-mail: chai.jat@kmutt.ac.th*
[4]*Professor, Department of Civil Engineering, Tokyo University of Science, 2641 Yamazaki, Noda, Chiba, 278-8510, Japan, Telephone: +81 4 7122 9819, Telefax: +81 4 7123 9766, E-mail: tatsuoka@rs.noda.tus.ac.jp*

Received 19 August 2011, revised 13 December 2011, accepted 4 January 2012

ABSTRACT: An automated tensile loading system that can accurately control histories of both loading and temperature was developed. A series of unconventional tensile loading tests were performed on polypropylene (PP), high-density polyethylene (HDPE) and polyester (PET) geogrids using this system. The following was found. The temperature significantly affects the elasto-viscoplastic stress–strain properties of the tested polymer geogrids. The inviscid stress–viscoplastic strain relation changes with temperature. The tensile rupture strength decreases by 9.2%, 26.7% and 4.5% when the temperature rises from 30°C to 50°C with PP, HDPE and PET geogrids, respectively. The elastic stiffness of the geogrid was evaluated by applying small-strain-amplitude unload–reload cycles after a certain period of sustained loading during otherwise monotonic loading at a constant load rate. The value increases with an increase in the tensile load level at a fixed temperature, and decreases with an increase in the temperature at a fixed load level. A set of mathematical expressions are proposed to describe these trends of tensile rupture strength and elastic behaviour.

KEYWORDS: Geosynthetics, Geogrid, Temperature, Tensile loading test, Rupture strength, Elastic stiffness, Three-component model

REFERENCE: Kongkitkul, W., Tabsombut, W., Jaturapitakkul, C. & Tatsuoka, F. (2012). Effects of temperature on the rupture strength and elastic stiffness of geogrids. *Geosynthetics International*, **19**, No. 2, 106–123. [http://dx.doi.org/10.1680/gein.2012.19.2.106]

1. INTRODUCTION

In current ordinary design practice, the design tensile strength of a given polymer geosynthetic reinforcement, V_d, is obtained by dividing the ultimate tensile strength obtained by performing a fast tensile loading test, V_{ult} (ASTM D4595; EN ISO 10319), by various reduction factors (RFs) (e.g. FHWA 2001) (Figure 1). As illustrated in Figure 1, these RFs are used: (1) to account for installation damage (RF_{ID}); (2) to account for long-term degradation (RF_D); and (3) to remove the possibility of creep failure (RF_{CR}). These reduction factors are also used in load and resistance factor design (LRFD), which is now recommended in North American design codes for reinforced-soil structures (e.g. Bathurst *et al.* 2011, 2012). The creep reduction factor (RF_{CR}) is generally determined by applying a specified design lifetime to the so-called 'creep–rupture curve'. This curve is typically obtained by performing a set of conventional creep tests (ASTM D5262), in which a set of time histories of tensile deformation at different constant tensile loads is obtained. However, this type of creep test is extremely time consuming. In particular, it is nearly impossible to perform these tests for an ordinary design lifetime of polymer geosynthetic reinforcement, say 50 years. For this reason, an accelerated creep test method (ASTM D6992; GRI 2000)

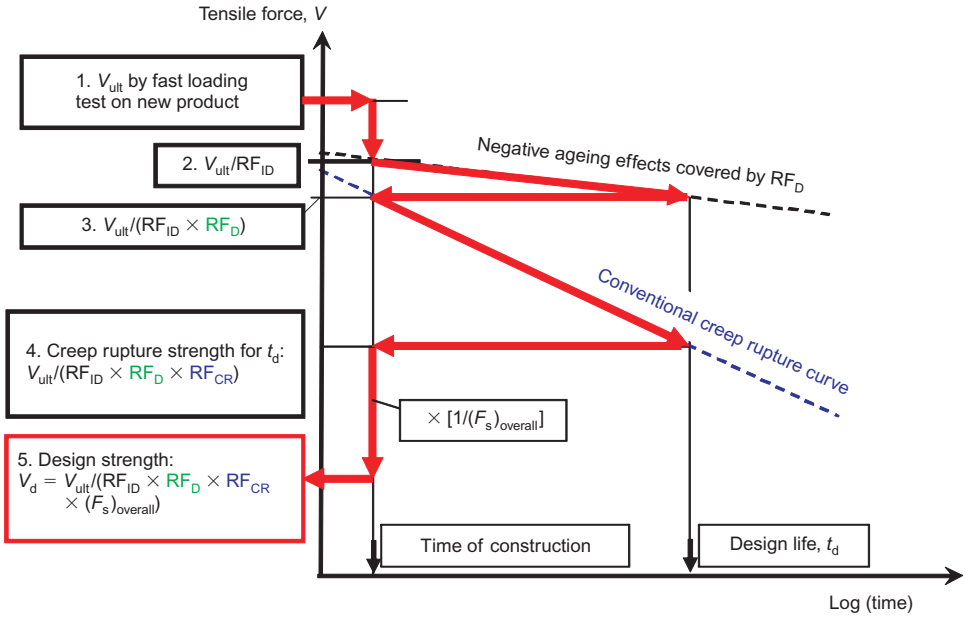

Figure 1. Method to obtain the design tensile strength of polymer geogrids (after Tatsuoka *et al.* 2004; Kongkitkul *et al.* 2007b).

was developed (e.g. Thornton *et al.* 1998), in which the temperature surrounding a test specimen is elevated to accelerate the creep strain rate. Then, based on analytical procedures (ASTM D6992; GRI 2000), a set of relationships between the tensile strain and the logarithm of time at the reference temperature for different tensile loads, called 'master curves', is obtained. From these relations, a creep–rupture curve at the reference temperature can be obtained. This technique is becoming popular, as evidenced by several studies on a wide variety of geosynthetic reinforcements (e.g. Thornton and Baker 2002; Greenwood *et al.* 2004; Zornberg *et al.* 2004; Bueno *et al.* 2005; Jones and Clarke 2006; Koo *et al.* 2006; Hsieh *et al.* 2006).

Figure 2a shows tensile load V plotted against strain ε for a polyester (PET) geogrid from four tests subjected to various loading histories (Hirakawa *et al.* 2003). In the first test, the V–ε relation (the solid line) changes significantly upon a step change in the strain rate, while significant creep deformation takes place during sustained loading, and significant load relaxation takes place at a fixed deformation. In the other three tests, monotonic loading (ML) towards ultimate failure was performed at three different constant strain rates (0.01%/min, 0.1%/min and 1.0%/min). Significant rate effects may be seen on the three V–ε relations. These trends of rate-dependent behaviour are due to the viscous properties of the tested geogrid. Figure 3a shows a similar result for high-density polyethylene (HDPE) geogrid. It may also be seen from Figure 3a that the V–ε relation exhibited very high stiffness, which is very similar to the elastic stiffness (k_{eq}), upon the restart of ML at a constant strain rate from the end of the respective load relaxation and sustained loading stages. These results indicate that the strength and deformation characteristics of polymer geosynthetic reinforcements are elasto-viscoplastic. In fact, as seen from Figures 2b and

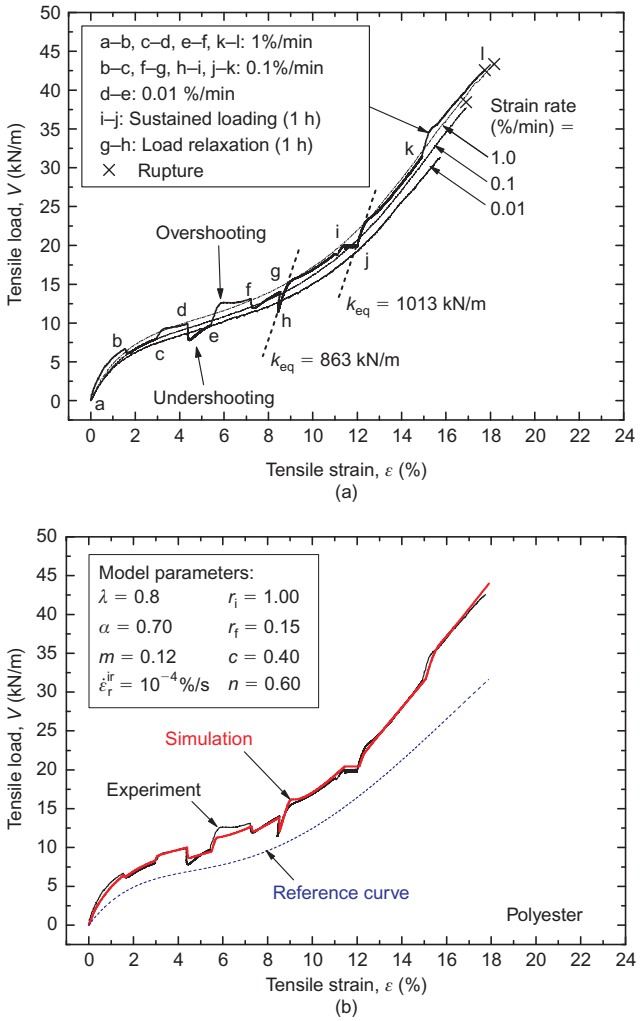

Figure 2. Elasto-viscoplastic tensile load–strain characteristics of a PET geogrid: (a) test results; (b) comparison of measured and simulated relations (modified from Hirakawa *et al.* 2003)

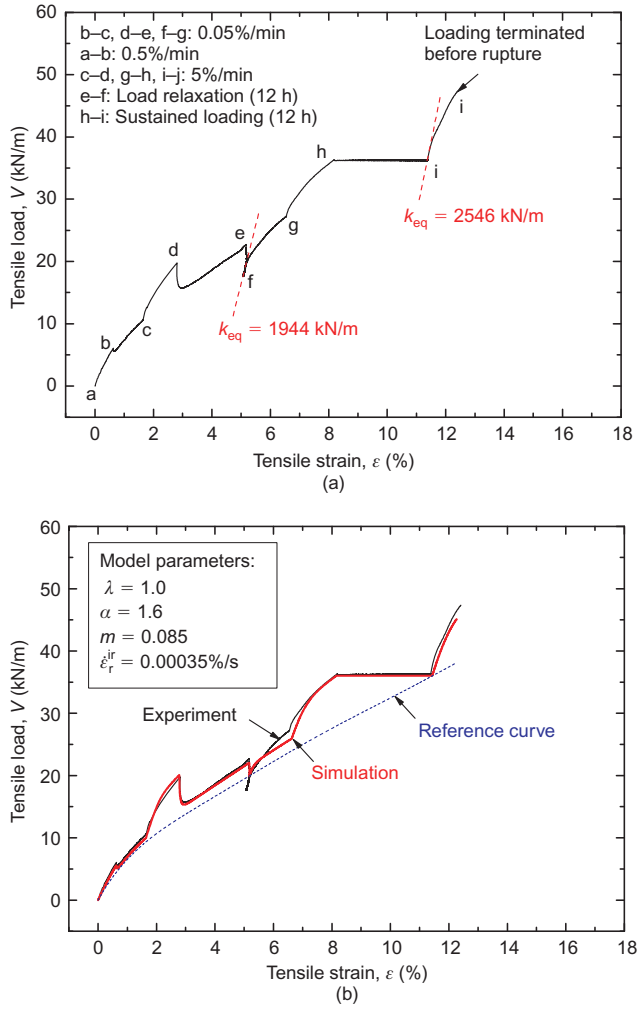

Figure 3. Elasto-viscoplastic tensile load–strain characteristics of an HDPE geogrid: (a) test results; (b) comparison of measured and simulated relations (modified from Hirakawa *et al.* 2003)

3b, these trends of rate-dependent behaviour can be accurately simulated by a non-linear three-component elasto-viscoplastic model (Figure 4) (e.g. Hirakawa *et al.* 2003; Kongkitkul *et al.* 2004, 2007a; Tatsuoka *et al.* 2004). Moreover, this model was successfully implemented to investigate the load–strain–time behaviours of polymer geogrids arranged in backfill soil (e.g. Kongkitkul *et al.* 2008, 2010b). In the framework of this model, the current tensile load V is decomposed into the inviscid tensile load V^f and the viscous tensile load V^v, and the current strain rate $\dot{\varepsilon}$ is decomposed into the elastic strain rate $\dot{\varepsilon}^e$ and the irreversible strain rate $\dot{\varepsilon}^{ir}$. According to this model, creep deformation is a response controlled by the viscous property of body V, not a degrading phenomenon. Long-term deterioration of the elastic stiffness of body E and the intrinsic tensile load–strain property of body P by chemical and/or biological reactions are treated as negative ageing effects in this model framework.

Figure 5 shows the V–ε relations for a woven polypropylene (PP) geotextile obtained from ML tests at a constant strain rate but at different ambient temperatures surrounding test specimens, as reported by Zornberg *et al.* (2004). Obviously, not only the ultimate strength but also the stiffness of the V–ε relation decreases with an increase in the temperature. These results are generally in agreement with the trends of behaviour of polymer geosynthetic reinforcements reported in the literature (e.g. Bush 1990; Shukla and Yin 2006). To simulate such temperature effects with the non-linear three-component model (Figure 4), Kongkitkul and Tatsuoka (2007) dealt with negative effects of a given time history of temperature increase on the strength and deformation characteristics of geosynthetic reinforcement as negative ageing effects, by which the strength and stiffness decrease with time.

Using the analogy explained above, Kongkitkul and Tatsuoka (2007) employed the non-linear three-component model to simulate the creep deformation of geosynthetic reinforcement that takes place at the same load when the temperature is increased in steps, under artificial (but typical) conditions. Figure 6a shows typical given time histories of tensile load and temperature and the time history of tensile strain (i.e. a given constant value in the range between a and b, followed by a response for the subsequent range); Figure 6b shows the simulated V–ε relation; and Figure 6c shows the time histories of total and irreversible tensile strains (simulated after point b). In this simulation, upon a step increase in the temperature,

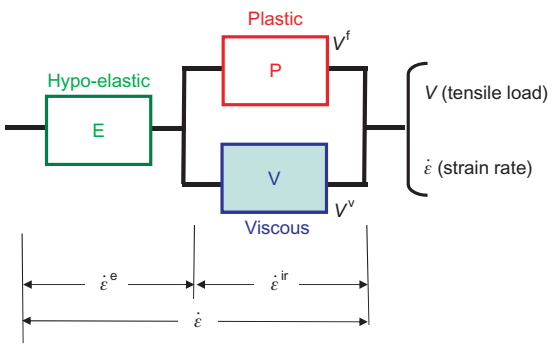

Figure 4. Non-linear three-component model for geosynthetic reinforcement (Hirakawa *et al.* 2003; Kongkitkul *et al.* 2004, 2007a, 2007b; Kongkitkul and Tatsuoka 2007)

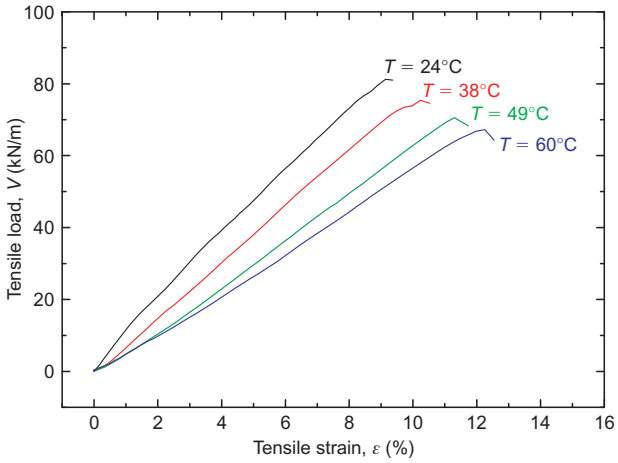

Figure 5. Tensile load–strain relations from monotonic loading tests on woven PP geotextile at different ambient temperatures (modified from Zornberg *et al.* 2004)

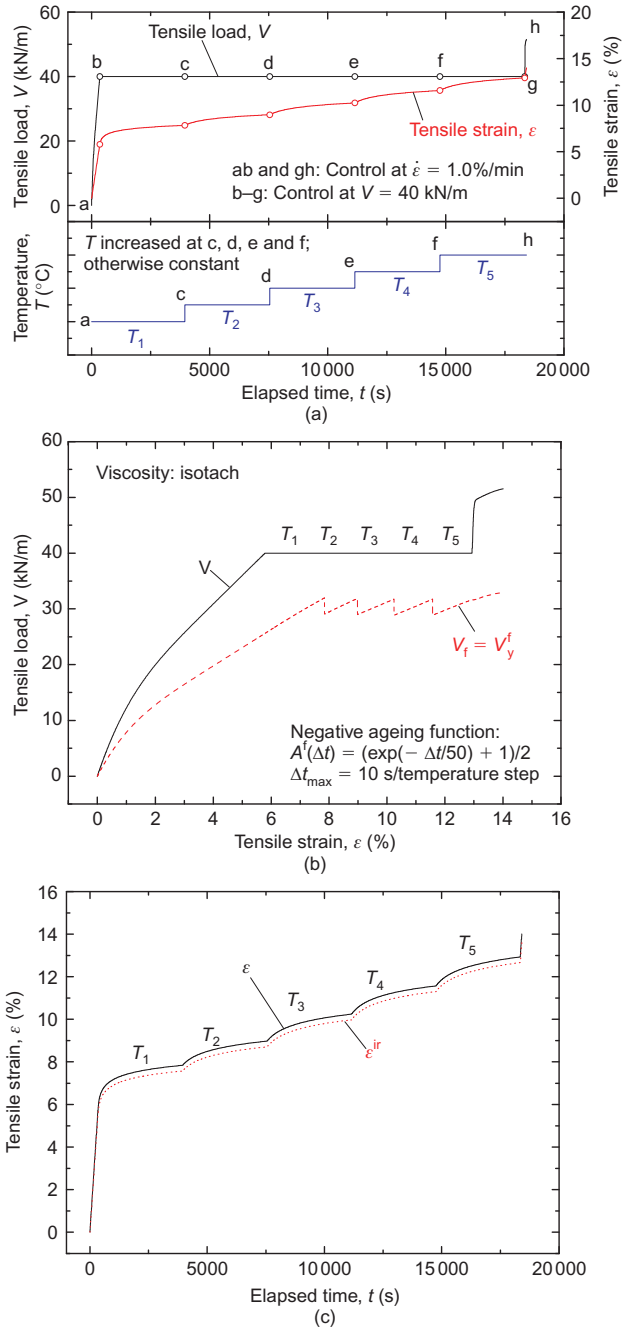

Figure 6. Numerical simulated results for SIM test at tensile load equal to 40 kN/m: (a) time histories of tensile load, tensile strain and temperature; (b) tensile load–strain relation; (c) time history of tensile strain (modified from Kongkitkul and Tatsuoka 2007)

the intrinsic tensile load V^f suddenly decreases, resulting in an acceleration of tensile strain rate. Subsequently, the tensile strain increases at a decreasing rate with time, while V^f increases towards the ultimate value, which is lower than the value at a lower temperature. In this analysis, both rate effects due to viscous properties (body V); and negative changes in the intrinsic tensile load–strain properties with temperature increase (body P) are taken into consideration. This analysis indicates that the model is potentially capable of simulating the load and deformation characteristics of polymer geosynthetic reinforcement affected by strain rate and temperature. Despite the above, the analysis presented in Figure 6 is approximate, as it was assumed that the elastic stiffness (body E) is independent of temperature. This approximation was introduced because little was known about the effects of temperature on the elastic stiffness of geosynthetic reinforcement when this analysis was performed.

In view of the above, for a systematic study into this issue, a series of unconventional tensile loading tests were performed on three different types of geogrid, commonly used in practice, by means of a newly developed tensile loading apparatus that can control the load rate and temperature precisely (Kongkitkul *et al.* 2010a).

2. TEST APPARATUSES AND MATERIALS

2.1. Test apparatus

The newly developed tensile loading apparatus (Figure 7) consists of two independent basic units for tensioning and heating. The tensioning unit is a slightly modified version of the one used by Kongkitkul *et al.* (2004, 2007a). It consists of an air cylinder, an air booster and an electro-pneumatic transducer to generate tensile forces applied to a specimen gripped with a pair of roller clamps (Hirakawa *et al.* 2003). The gripped specimen is placed inside a temperature-controlled chamber 50 cm wide by 35 cm deep by 64 cm high. The chamber comprises plywood plates with polyethylene (PE) foam insulator glued on both faces. Both sides of the PE foam insulator are laminated with 8 μm-thick pure aluminium foil. First, the top sheet of aluminium foil reflects heat radiation, and then the PE foam provides insulation against heat from conduction and convection. Finally, the bottom sheet of aluminium foil protects the bottom air layer of the insulator from heat radiation more effectively. A tempered glass panel is installed at the front of the chamber for observation of specimens during testing (Figure 8). Various loading histories, including monotonic loading at different load rates, sustained loading at different loads and load reversing at arbitrary moments can be accurately applied by precisely controlling the tensioning unit by means of a personal computer.

The heating unit consists of a blower, a heater, a feedback-controllable controller and a network of air pipes (Figure 7). Its working principle is as follows. Air is first supplied to the blower and then transferred to the heater. Hot air is provided to a temperature-controlled chamber via an air pipe arranged at the bottom, and moves inside a perforated air pipe arranged inside the chamber. The heat from the hot air is well distributed by means of a set of fans. Finally, the hot air exits from the top of the chamber. Half of the hot air that comes out from the top of the chamber is exhausted, and the other half is sent to the blower, where the circulated hot air is mixed with the newly provided air at the room-temperature in a volume ratio of 1:1, so that the temperature distribution inside the chamber becomes uniform efficiently. This was confirmed by the fact that the maximum difference among readings

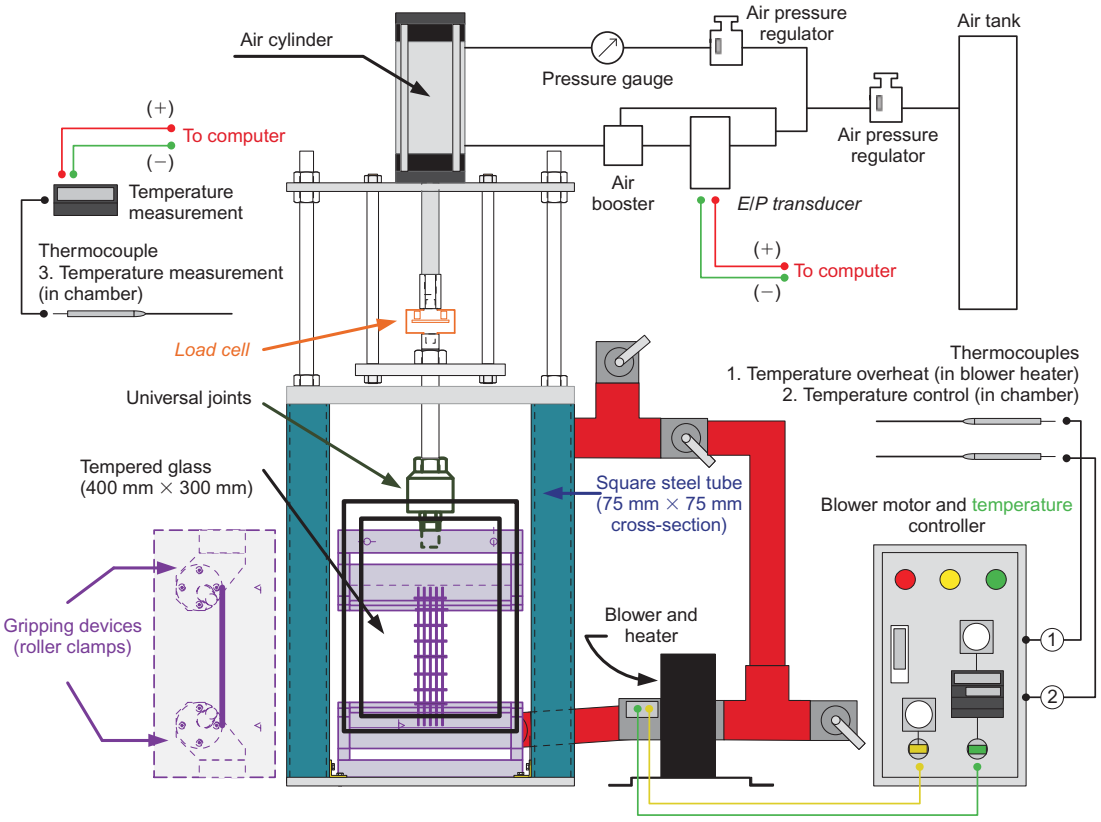

Figure 7. Details of temperature- and load-controlled tensile loading apparatus used in this study

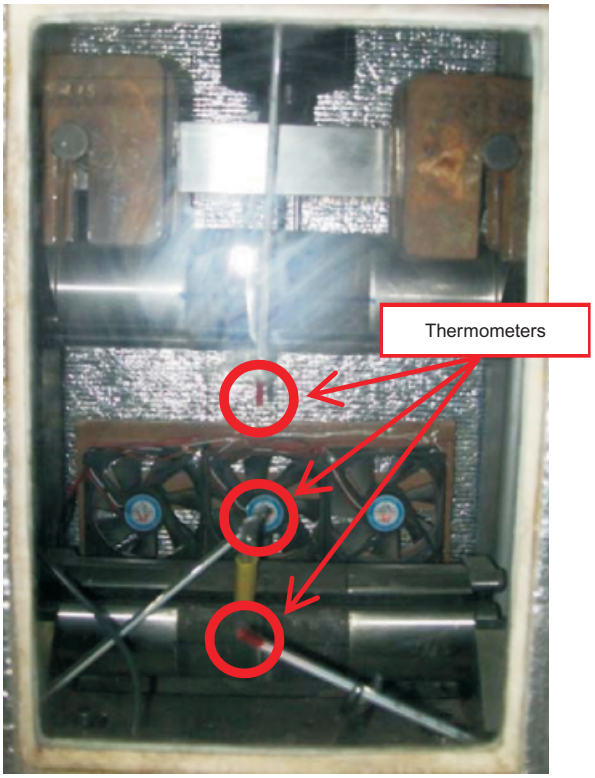

Figure 8. Installations of thermometers to investigate temperature distribution inside the chamber

of thermometers installed at three locations along the length of the specimen inside the chamber (Figure 8) was less than 1.0°C. The reading from a thermocouple installed inside the chamber (thermocouple 2 in Figure 7) was used to control the chamber temperature by means of a controller. By using this heating unit, the temperature histories, including processes of increasing and decreasing at given rates as well as constant temperature, can be precisely controlled. The chamber temperature was measured with another thermocouple installed in the chamber, next to the one described above, (thermocouple 3 in Figure 7) and recorded by the personal computer. Figure 9 shows a typical measured time history of chamber temperature. It can clearly be seen that the measured temperature follows the target value fairly precisely, showing that the heating unit can successfully control a given arbitrary temperature history.

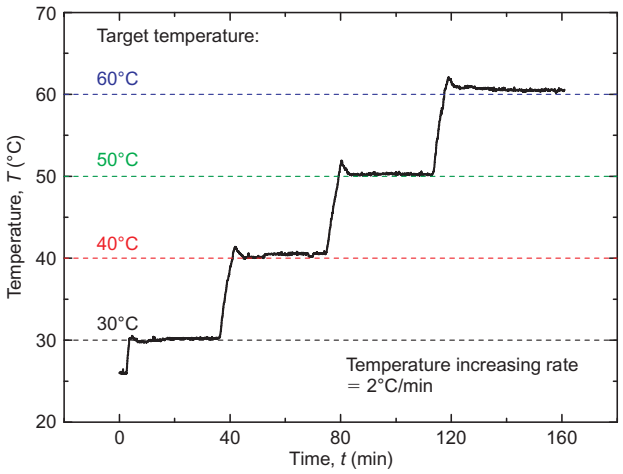

Figure 9. Typical time history of measured temperature inside the temperature-controlled chamber

2.2. Test materials and specimen preparations

Three different types of polymer geogrid were used (Figure 10): polypropylene (PP), high-density polyethylene (HDPE) and polyester (PET). Table 1 lists the physical, dimensional and technical characteristics of these geogrids, as provided by their respective manufacturers.

Before the start of tensile loading, the specimen, which consisted of either three strands for the PP and HDPE geogrids or four strands for the PET geogrid (Figure 10), was wrapped around the roller clamps and locked to the grooves with steel rods. The initial test length of the specimen was approximately 24 cm. A pre-tension of 20 N was applied to the specimen to minimise bedding errors between the surface of the roller clamps and the attached specimen. The two side strands were removed by cutting to obtain a single-strand specimen of the PP and HDPE geogrids and a two-strand specimen of the PET geogrid (Figure 10). A small frame guided by two vertical rods holding an LVDT and a target (Figure 10) was attached to the specimen to measure the local tensile strain, with an initial measuring gauge length of 3 cm. This small frame was designed to minimise the effects of rotation around the vertical axis (i.e. the z-axis in Figure 10) and the two horizontal axes (i.e. the x- and y-axes) that might occur during a strain-measurement test. The safe temperature range of the LVDT used is from -10°C to 70°C (non-condensing), according to the manufacturer's technical data. As the total weight of this small frame, together with an LVDT, is only 3 N, the effects of its weight on the measured tensile strain value should be negligible. The PET geogrid specimen consisted of two strands rather than a single strand. This is because the width and thickness of a single strand were too small for the small frame for local tensile strain measurement to grip, and PET geogrid is much easier to bend and twist than PP and HDPE geogrids. As a result, rotation around the y- and z- axes tended to occur when a single-strand specimen was used. This was not the case with the PP or HDPE geogrids.

2.3. Tensile loading and temperature histories

After having arranged the small frame to measure tensile strains, the front plate of the chamber was installed to form the test chamber. The temperature inside the chamber was increased at a rate of 2°C/min until the target temperature was reached. It was then held constant at the target value for 2 h, to allow the specimen to settle at the elevated temperature. The tensile strain was defined as

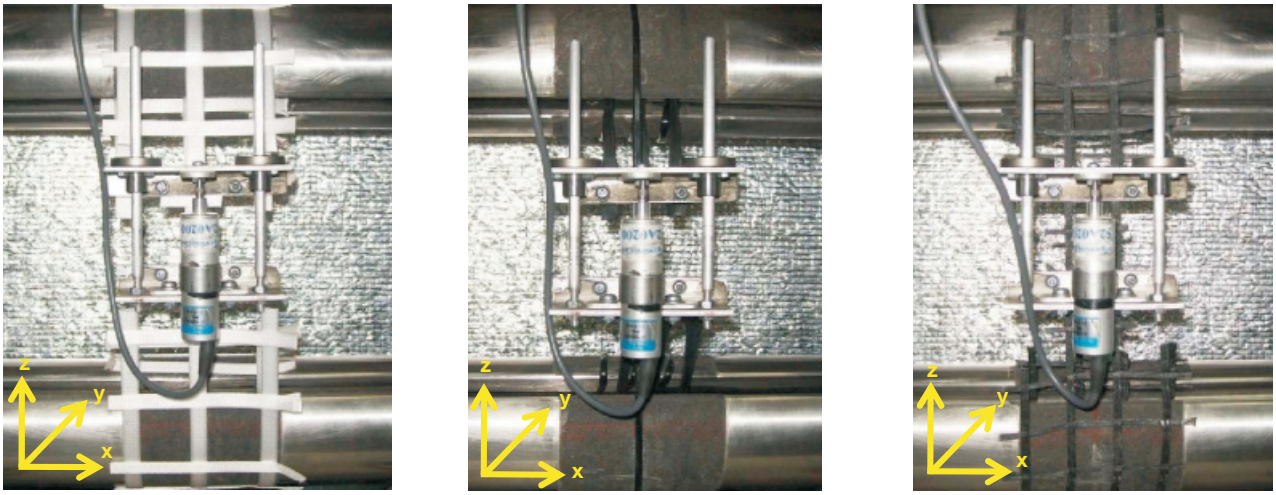

Figure 10. Specimens gripped with roller clamps and installed with a small frame for local deformation measurement: (a) PP geogrid; (b) HDPE geogrid; (c) PET geogrid

Table 1. Physical, dimensional and technical characteristics of geogrids used in this study

Characteristic	Fibre material		
	Polypropylene	High-density polyethylene	Polyester
Abbreviated name	PP	HDPE	PET
Standard colour	White	Black	Black
Specimen conditions	Virgin	Virgin	Virgin
Aperture size (MD/TD)[a] (mm)	35/35	220/16	25/25
Max tensile strength (MD/TD) (kN/m)	⩾80/⩾80	90/–	80/30
Yield point elongation (MD) (%)	⩽8	13	11

[a]MD = machine direction (longitudinal to roll)/TD = transverse direction (across roll width)

zero, and the tensile load was then increased, following predefined loading histories (explained below), while the temperature was kept constant throughout the loading scheme. The target temperatures selected in this study were different for different types of geogrid, as listed in Table 2, but a common reference temperature of 30°C was selected. The following two loading histories were employed.

1. Monotonic loading (ML) was continued at a load rate ($\dot{V}$) of 0.6 kN/m/min until ultimate rupture.
2. During otherwise ML at a constant load rate, 10 small-amplitude unload–reload cycles with a double amplitude of 2 kN/m were also applied at a load rate ($\dot{V}$) of ±0.6 kN/m/min immediately after 3 h sustained loading at four tensile load levels to determine the elastic stiffness at different load levels and different temperatures.

3. TEST RESULTS AND DISCUSSION

3.1. Effects of temperature on rupture strength

Figures 11a, 11b and 11c show the relationships between the tensile load V and the tensile strain ε obtained by continuous ML at a constant load rate of 0.6 kN/m/min performed at different temperatures towards the peak strength (loading history a) using PP, HDPE and PET geogrids, respectively. In all the tests on the PP and PET geogrids, loading was ended when the specimen exhibited tensile rupture: so the maximum tensile load V_{max} was exhibited at the end of the test (indicated by the symbol × in Figures 11a and 11c). With the HDPE geogrid, on the other hand, tensile rupture did not occur by the end of test (indicated by the symbol +), owing to the tensile deformation capacity of the apparatus. Consequently, for the V–ε relations of the HDPE geogrid, the yield point (which is seemingly not largely different from the rupture point), was obtained (indicated by the symbol × in Figure 11b), because the tensile load at the end of loading is not objective. To obtain the yield point in an objective way, it was defined as the location along the V–ε relation at which the radius of curvature ρ becomes the minimum in the log V–log ε relation, as typically shown in Figure 12. The radius of curvature ρ in each test was obtained numerically, so that the obtained yield point was not subjective. This technique has been used to determine yield stresses at different confining pressures in drained triaxial compression tests on geomaterials employing multiple loading histories to define a yield surface (e.g. Nawir *et al.* 2003; Ezaoui *et al.* 2010). In the following,

Table 2. Tested ambient temperatures selected in this study

Geogrid type	Tested ambient temperatures (°C)
Polypropylene (PP)	30, 35, 40, 45, 50
High-density polyethylene (HDPE)	30, 35, 40, 45, 50
Polyester (PET)	30, 40, 50

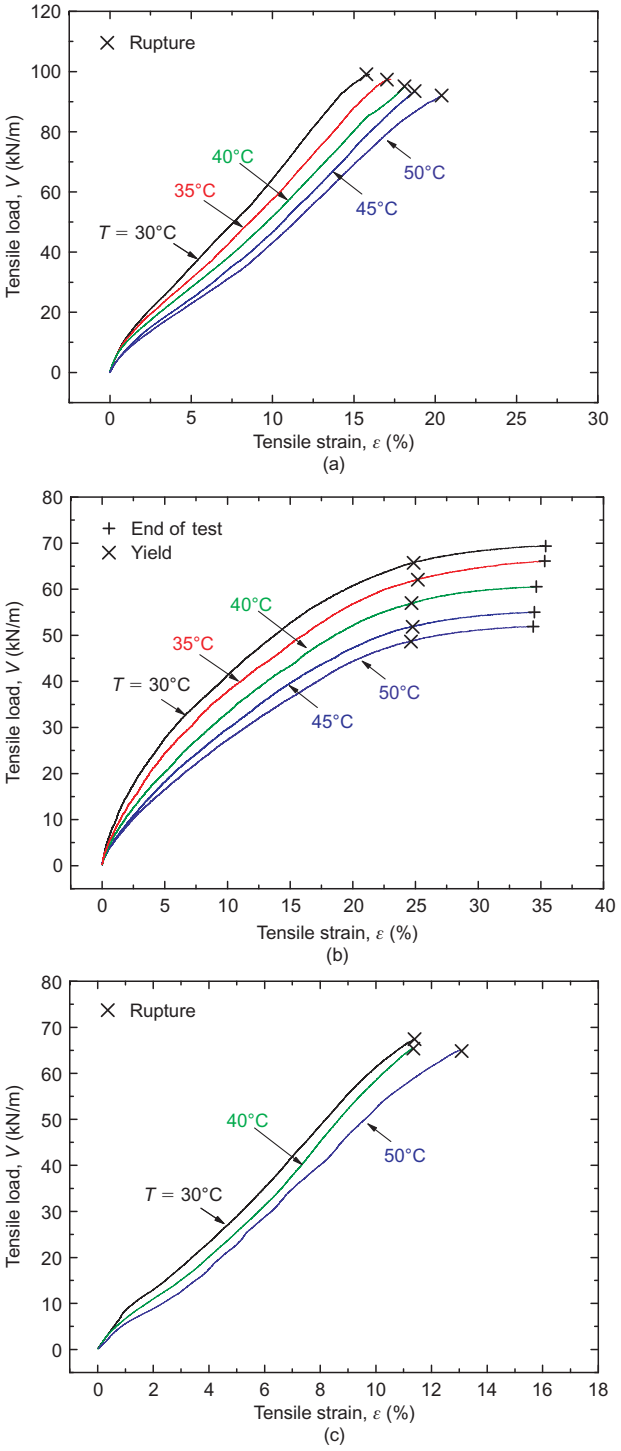

Figure 11. Tensile load–strain relations from continuous ML tests at load rate of 0.6 kN/m/min until rupture at different constant temperatures: (a) PP geogrid; (b) HDPE geogrid; (c) PET geogrid

with the HDPE geogrid, the tensile load at the yield point for each temperature was treated as the rupture strength V_{max}. Therefore the true rupture strength is slightly higher than the value of V_{max} obtained as above. The measured values of V_{max} for the three geogrid types, denoted as original V_{max}, are summarised in Table 3. It may be seen from Figures 11a–11c that not only the rupture strength but also the stiffness decreases with an increase in the temperature. This test result indicates that an increase in

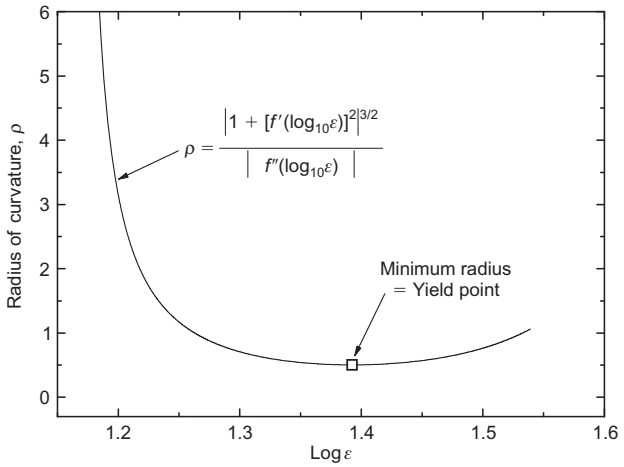

Figure 12. Relation between radius of curvature of log(tensile load)–log(tensile strain) relation and logarithm of tensile strain, from continuous ML test on HDPE geogrid at temperature of 40°C

the temperature surrounding the tested geogrids results in negative effects on the intrinsic load–strain properties (represented by body P in Figure 4). Yet we cannot know from these test results whether or how the elastic modulus of body E (Figure 4) decreases with an increase in temperature. This issue is discussed in detail later in this paper.

The load rate, $\dot{V}$, was kept the same and constant (= 0.6 kN/m/min) in these tests performed at different temperatures, as described in Figures 11a–11c. The strain rate at rupture, $\dot{\varepsilon} = \dot{V}/k_{\tan}$, increases with an increase in the temperature, because of a decrease in the tangent stiffness $k_{\tan}$ of the V–ε relation. Therefore, to evaluate the pure effects of temperature, the rupture strengths observed at different strain rates presented in Figures 11a–11c (i.e. the original $V_{\max}$ values listed in Table 3) were corrected to the values at the same strain rate (i.e. 0.1%/m) as follows.

With geosynthetic reinforcement, upon a stepwise increase or decrease in the strain rate, the tensile load suddenly jumps or drops. Figure 13 shows the relationships between the normalised tensile load jump $\Delta V/V$ and the logarithm of the ratio of strain rates after and before a step change of several typical geosynthetic reinforcement types, including those tested in the present study. These test results were obtained from previously performed series of experiments (Hirakawa *et al.* 2003; Kongkitkul *et al.* 2004, 2007b), in which the strain rate was changed stepwise many times during otherwise ML at constant strain rates (e.g. Figures 2a and 3a). The rate-sensitivity coefficient β is defined such that the jump or drop of tensile load from the current tensile load V on a tenfold increase or decrease in the strain rate is expressed as $\Delta V = \beta \times V$ (Di Benedetto *et al.* 2002; Hirakawa *et al.*

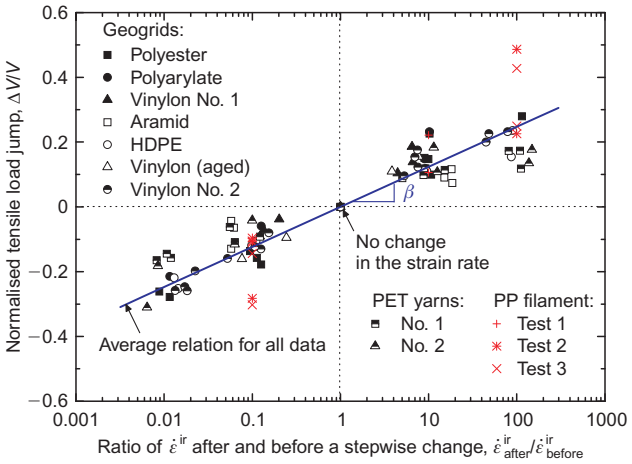

Figure 13. Rate-sensitivity coefficients of various types of geosynthetic reinforcement and a polypropylene (PP) filament (modified from Kongkitkul *et al.* 2007b)

Table 3. Comparisons of rupture strengths at different temperatures: original values and those corrected to $\dot{\varepsilon} = 0.1$%/min

Geogrid type	T (°C)	Original $V_{\max}$ (kN/m)	Strain rate (%/min)	Corrected $V_{\max}$ (kN/m)[a]
Polypropylene (PP)	30	99.14	0.098	99.30
	35	97.31	0.110	96.39
	40	95.11	0.114	93.85
	45	93.48	0.115	92.19
	50	92.04	0.122	90.16
High-density polyethylene (HDPE)[b]	30	65.76	0.659	59.66
	35	62.05	0.608	56.55
	40	56.98	0.653	51.72
	45	51.86	0.791	46.58
	50	48.62	0.768	43.75
Polyester (PET)[c]	30	67.43	0.086	67.92
	40	65.39	0.083	66.00
	50	64.86	0.100	64.86

[a] Corrections were made to obtain the respective $V_{\max}$ at $\dot{\varepsilon} = 0.1$%/min.
[b] Tensile loads at yield points, treated as rupture strengths, of HDPE geogrid.
[c] Lightly non-isotach viscous property. $V_{\max}$ corrected based on results from continuous ML tests at different strain rates.

2003; Kongkitkul *et al.* 2004). The line shown in Figure 13 was obtained to best-fit all the data points, and its slope indicates the average β value for all the geosynthetic reinforcement types. The β value for each geosynthetic reinforcement type was determined from the slope of a line best-fitted to the respective data set shown in Figure 13. The values of β for HDPE and PET geogrids, determined as above, are reported by Kongkitkul *et al.* (2007b), and the value for PP geogrid is reported by Shinoda *et al.* (2002). These β values are listed in Table 4. As reported by Kongkitkul *et al.* (2007b), the β values of polymer geogrids manufactured from the same type of polymer are nearly the same.

In addition, it is known that the rate-dependent V–ε behaviour of most polymer geosynthetic reinforcements is of the isotach type (Hirakawa *et al.* 2003; Tatsuoka *et al.* 2004; Kongkitkul *et al.* 2004, 2007a). Only PET geogrid exhibits slight non-isotach behaviour (Figure 2a). With the isotach viscous property type, the current viscous tensile load V^{v} is a unique function of the current irreversible strain $\varepsilon^{\mathrm{ir}}$ and its rate, $\dot{\varepsilon}^{\mathrm{ir}}$. As the current inviscid tensile load V^{f} is a unique function of the current irreversible strain, $\varepsilon^{\mathrm{ir}}$, and is independent of its rate, $\dot{\varepsilon}^{\mathrm{ir}}$, the change in the tensile load ($V = V^{\mathrm{f}} + V^{\mathrm{v}}$) caused by a change in the strain rate is equal to a change in V^{v}. Consequently, the change in the tensile load caused by a change in the strain rate is persistent as long as $\dot{\varepsilon}^{\mathrm{ir}}$ is kept the same during subsequent loading after a step change in the strain rate. Table 3 lists the strain rates at rupture in the various tests shown in Figures 11a–11c. For the PP and HDPE geogrids (which exhibit isotach viscosity), as listed in Table 3, the original $V_{\max}$ values were corrected to those at a strain rate of 0.1%/min by using the respective β values (listed in Table 4) and the ratio of the strain rate measured at rupture to 0.1%/min. Note that the β values listed in Table 4, which are taken from previous research, were used in the above-mentioned correction. The β values of these polymer reinforcements were not obtained in the present study, because it is not possible to change the strain rates in stepwise fashion under well-controlled conditions in the present study using a load-controlled tensile loading apparatus. With the same polymer geosynthetic reinforcement types, the batches used in this study are different from those used in the previous studies. However, Kongkitkul *et al.* (2007b) showed that the β values of different batches of the same type of polymer geosynthetic reinforcement are very similar. Only with PET geogrid is the viscous property type not of isotach type: that is, only 80% of the ΔV that develops upon a strain rate change is maintained during subsequent continuous ML at a constant strain rate. This trend implies the use of $\beta = 0.1142$ (80% of the original value, 0.1428) when correcting the original $V_{\max}$ values for strain-rate effects assuming isotach viscous properties, as for the PP and HDPE geogrids.

3.2. Temperature effect parameter

The temperature effect on the tensile rupture strength at the same strain rate (= 0.1%/min) can be represented by the relationship between the temperature effect parameter A^{f}, defined as the ratio of $V_{\max}$ (i.e. the strength at a given temperature, T) to $V_{\max 0}$ (i.e. the value at the reference temperature, $T_0 = 30^{\circ}\mathrm{C}$) and the temperature T, where $V_{\max}$ and $V_{\max 0}$ are the values at a strain rate equal to 0.1%/min. Figures 14a–14c show these relations for PP, HDPE and PET geogrids, respectively. The parameter A^{f} decreases with an increase in the temperature T. In these figures, the $V_{\max}/V_{\max 0}$ ratios obtained from the original $V_{\max}$ values measured at different strain rates are also shown, for reference. It may be seen that the data are fitted very well by the equation

$$A^{\mathrm{f}} = \frac{V_{\max}}{V_{\max 0}} = 1 - a\left(\frac{T - T_0}{T_0}\right)^b, \quad T \geqslant T_0 \tag{1a}$$

where a and b are constants, the values of which are shown for the various types of geogrid in Figures 14a–14c. Equation 1b expresses an axisymmetric relation of Equation 1a that is assumed to be relevant only when $T < T_0$ (= 30°C). This equation is used below to extrapolate the values measured at T higher than T_0 to those for T lower than T_0.

$$A^{\mathrm{f}} = \frac{V_{\max}}{V_{\max 0}} = 1 + a\left(\frac{T_0 - T}{T_0}\right)^b, \quad T < T_0 \tag{1b}$$

Tensile loading tests are usually performed at 20°C in many countries (EN ISO 10319; ASTM D4595), which is herein called the standard temperature, denoted as T_0'. In this study, however, the basic temperature used (called the reference temperature, denoted as T_0) is equal to 30°C. This is because a cooling system is necessary to achieve a constant temperature of 20°C in Bangkok (where this study was performed). Equation 1b was used to extrapolate the A^{f} values measured at $T \geqslant T_0$ to the values at $T = 20^{\circ}\mathrm{C}$ and 25°C for the PP and HDPE geogrids and the value at $T = 20^{\circ}\mathrm{C}$ for the PET geogrid. These extrapolated A^{f} values are larger than unity, as listed in Table 5. Although Equation 1b has not been validated, as the extent of these extrapolations is small, it is deemed that the use of Equation 1b results in only a very small error, if any. The rupture strength at $T_0' = 20^{\circ}\mathrm{C}$, $V'_{\max 0}$, was back-calculated as the rupture strength at $T_0 = 30^{\circ}\mathrm{C}$ times the A^{f} value at $T_0' = 20^{\circ}\mathrm{C}$. Then the relationships between the temperature effect parameter $A^{\mathrm{f}\prime}$ (defined as the ratio of

Table 4. Rate-sensitivity coefficients of the geogrids used in this study

Geogrid type	β	Reference
Polypropylene (PP)	0.2326	Shinoda *et al.* (2002)
High-density polyethylene (HDPE)	0.1132	Kongkitkul *et al.* (2007b)
Polyester (PET)	0.1428	Kongkitkul *et al.* (2007b)

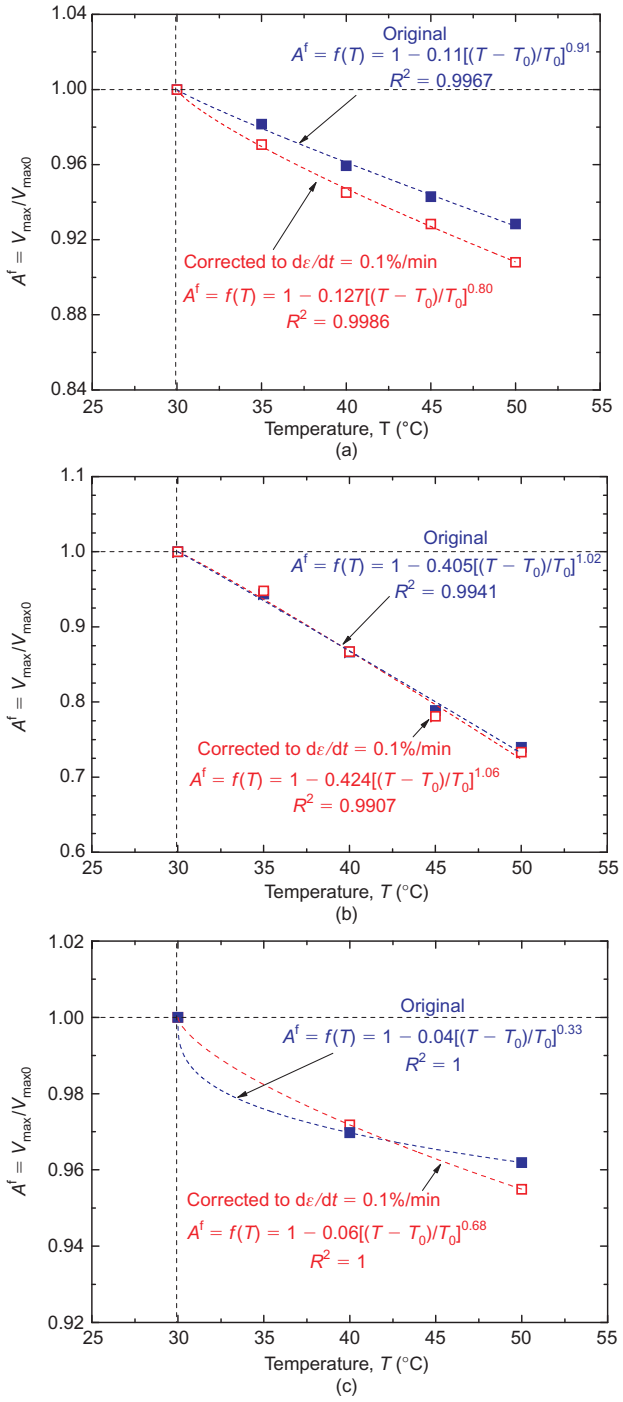

Figure 14. Temperature effect parameter A^f as a function of temperature T, defined for the reference temperature $T_0 = 30°C$ for: (a) PP geogrid; (b) HDPE geogrid; (c) PET geogrid

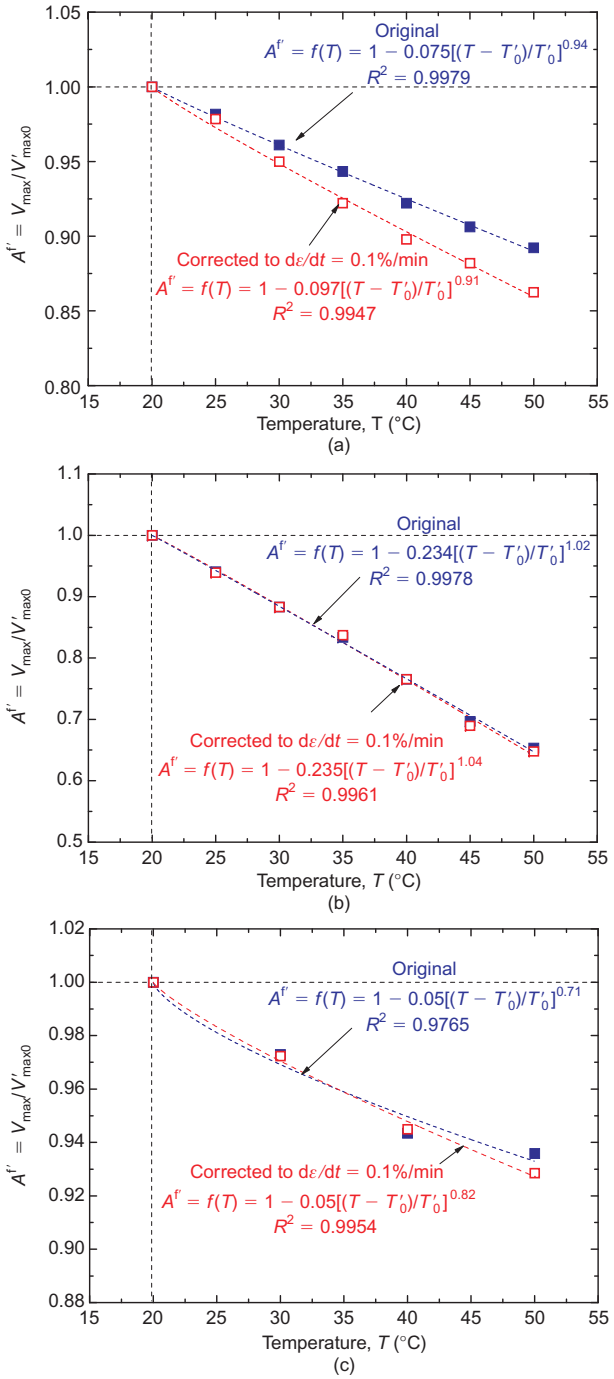

Figure 15. Temperature effect parameter $A^{f\prime}$ as a function of temperature T, defined for the standard temperature $T'_0 = 20°C$ for: (a) PP geogrid; (b) HDPE geogrid; (c) PET geogrid

V_{max}, the rupture strength at a given temperature, to V'_{max0}, the value at $T'_0 = 20°C$), and the temperature T for the PP, HDPE and PET geogrids were obtained (Figures 15a–15c). The parameter $A^{f\prime}$ decreases with an increase in the temperature T. Then, Equation 2 was fitted to the data, as with Equation 1a.

$$A^{f'} = \frac{V_{max}}{V'_{max0}} = 1 - a'\left(\frac{T - T'_0}{T'_0}\right)^{b'}, \quad T \geqslant T'_0 \qquad (2)$$

where a' and b' are constants, the values of which are shown for the various types of geogrid in Figures 15a–c.

3.3. Tensile load–strain relations during cyclic loading

Figures 16a–16c show the V–ε relations from tests performed following loading history b at different constant temperatures. Ten unload–reload cycles of tensile load with a small load amplitude (2 kN/m) were applied at the tensile loads (V) listed in Table 6. Following the technique that has been widely used to determine the elastic proper-

Table 5. Temperature effect parameters A^f and $A^{f\prime}$ defined, respectively, for reference temperature $T_0 = 30°C$ and standard temperature $T_0' = 20°C$

Geogrid type	T (°C)	Original V_{max}			Corrected V_{max}		
		A^f	V_{max} (kN/m)	$A^{f\prime b}$	A^f	V_{max} (kN/m)	$A^{f\prime b}$
Polypropylene (PP)	20	1.041[a]	103.15[a]	1.000	1.053[a]	104.54[a]	1.000
	25	1.021[a]	101.27[a]	0.982	1.030[a]	102.28[a]	0.978
	30	1.000	99.14	0.961	1.000	99.30	0.950
	35	0.982	97.31	0.943	0.971	96.39	0.922
	40	0.959	95.11	0.922	0.945	93.85	0.898
	45	0.943	93.48	0.906	0.928	92.19	0.882
	50	0.928	92.04	0.892	0.908	90.16	0.862
High-density polyethylene	20	1.132[a]	74.44[a]	1.000	1.132[a]	67.56[a]	1.000
(HDPE)	25	1.065[a]	70.04[a]	0.941	1.063[a]	63.45[a]	0.939
	30	1.000	65.76	0.883	1.000	59.66	0.883
	35	0.944	62.05	0.834	0.948	56.55	0.837
	40	0.867	56.98	0.765	0.867	51.72	0.766
	45	0.789	51.86	0.697	0.781	46.58	0.690
	50	0.739	48.62	0.653	0.733	43.75	0.648
Polyester (PET)	20	1.028[a]	69.31[a]	1.000	1.028[a]	69.85[a]	1.000
	30	1.000	67.43	0.973	1.000	67.92	0.972
	40	0.970	65.39	0.943	0.972	66.00	0.945
	50	0.962	64.86	0.936	0.955	64.86	0.929

[a] Extrapolated by Equation 1b.
[b] Expressed by Equation 2 for standard temperature $T_0' = 20°C$

ties of geomaterials reliably by triaxial tests (e.g. Shibuya *et al.* 1992; Tatsuoka *et al.* 1994; Hoque and Tatsuoka 1998), sets of 10 small unload–reload cycles were applied after sustained loading (SL) had been applied for 3 h. It was expected that the tensile load–strain behaviour during cyclic loading (CL) would become essentially elastic by this method.

3.4. Determination of elastic stiffness

Figure 17 shows data obtained at the lowest load level at the respective temperatures of PP geogrid, which is typical of those obtained by the present study. In these cases, the behaviour during small unload–reload cycles is highly linear-elastic, as noted by the facts that: (1) the load–strain loops generated during the respective unload–reload cycles are very small, exhibiting negligible energy dissipation; and (2) the residual strain developed by the respective unload–reload cycles was very small. As shown in Figures 18a–18e, the unloading V–ε branches exhibit highly linear-elastic behaviour for a large range of tensile load increments relative to the whole load amplitude (2 kN/m). Thus it is relevant to evaluate the equivalent elastic stiffness k_{eq} from a linear relation fitted to the respective portions of the unloading V–ε branches presented in Figure 18. Although the data are scattered to some extent, as can be seen from Figure 19, the k_{eq} values can be defined with a degree of confidence. The value of k_{eq} is fairly constant during 10 unload–reload cycles for the respective CL stages. This fact indicates that the deformation during these unloading V–ε branches is essentially elastic.

However, the range of tensile load increments over which the unloading V–ε branches exhibit highly linear-elastic behaviour decreases significantly as the load level increases, and as the temperature increases. This is because the residual strains that develop during unload–reload cycles at high load levels, particularly at high temperatures, are not negligible, as can be seen from Figures 16a–16c. This trend can be clearly seen by comparing Figure 20a with Figure 20b. In these cases it is therefore necessary to find a portion of the whole load–strain behaviour that exhibits essentially elastic behaviour (i.e. rate-independent and reversible) during the respective unload–reload cycles.

Figures 21a–21d shows data typical of cases in which the V–ε behaviour is highly linear and reversible only for a small range of tensile load increment near the bottom end of the V–ε loop. In these figures, the unloading V–ε branches are presented for a small range near the bottom end of the full ranges by CLs with a load amplitude of 2 kN/m at the highest load levels of the respective tests at different temperatures performed on PP geogrid. Figure 21e shows a similar result at the second highest load level at $T = 50°C$. The behaviour shown in these figures can be deemed essentially reversible (and therefore elastic), as can be seen from Figure 20b. The load amplitude for these selected bottom ranges, presented in Figure 21, is much smaller than those at a lower load level and at a lower temperature (Figure 18). The above-mentioned trends of behaviour were also observed during CLs on the HDPE and PET geogrids. A linear relation was fitted to the bottom range of the respective unloading V–ε branches presented in Figure 21 to obtain k_{eq}. As seen from Figure 21, in this case also the value of k_{eq} is fairly constant during 10 unload–reload cycles at the respective CL stages.

The k_{eq} values at the load levels listed in Table 6 and temperatures listed in Table 2 of the PP geogrid (other

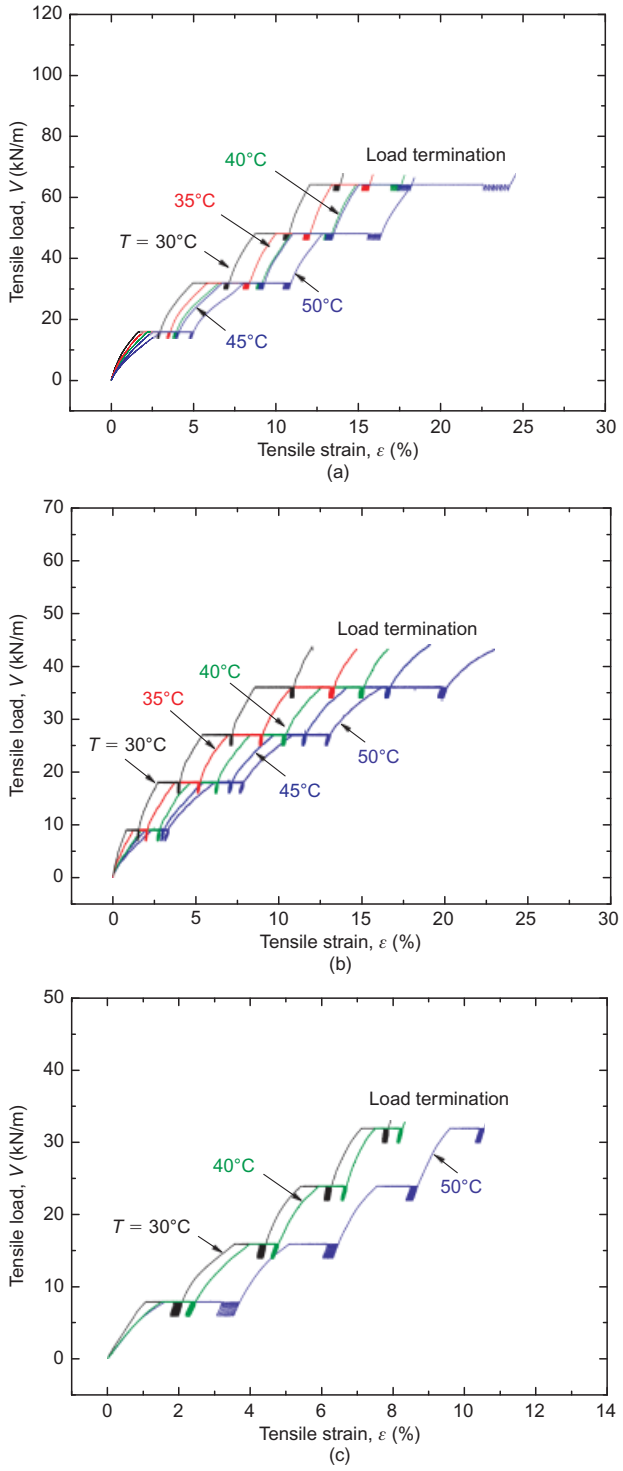

Figure 16. Tensile load–strain relations from ML with small-amplitude unload–reload cycles at various tensile load levels under different constant temperatures: (a) PP geogrid; (b) HDPE geogrid; (c) PET geogrid

than those presented in Figures 18 and 21), and those of the HDPE and PET geogrids, were determined in the same way, as shown in Figures 18 and 21.

3.5. Effects of temperature on elastic stiffness

Among 10 measured values of k_{eq} at the respective CL stages for different combinations of load level and temperature (as shown in Figures 18 and 21), the lowest two and the highest two values were excluded, and the average k_{eq} was determined from the six remaining values. Figures 22a–22c show the relationships between the average k_{eq} value and the load level (V/V_{max}) in a full-log plot for the PP, HDPE and PET geogrids, respectively, where V_{max} is the rupture strength corrected to $\dot{\varepsilon} = 0.1\%$/min. The following trends of behaviour may be seen.

Table 6. Tensile loads at which small-amplitude cyclic loading was performed on the three types of geogrid

Geogrid type	Tensile load, V (kN/m)
Polypropylene (PP)	16, 32, 48, 64
High-density polyethylene (HDPE)	9, 18, 27, 36
Polyester (PET)	8, 16, 24, 32

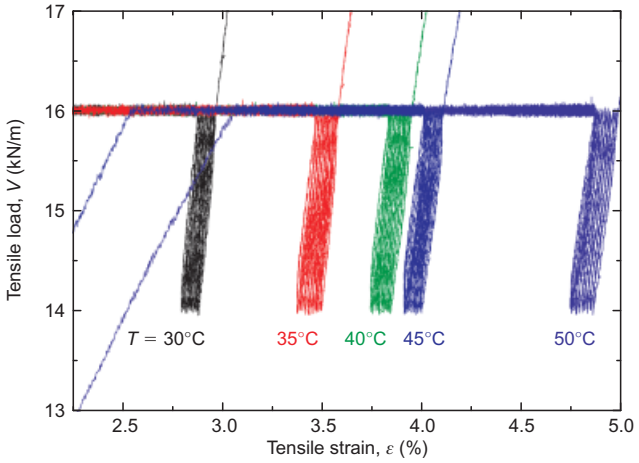

Figure 17. Enlarged V–ε relation of PP geogrid at lowest load level at different temperatures presented in Figure 16a

1. At the respective constant temperatures, the k_{eq} value increases significantly with an increase in the load level. Moreover, the slope of the linear relation is insensitive to temperature for all the tested geogrid types. These trends indicate that the tested geogrids have specific hypo-elastic properties. With respect to the hypo-elastic properties, the trend that the elastic stiffness of geomaterial increases with an increase in the major principal stress for which the elastic modulus is defined has been observed in triaxial tests of many types of unbound geomaterial (e.g. Shibuya *et al.* 1992; Tatsuoka *et al.* 1994; Hoque and Tatsuoka 1998). On the other hand, it is not well understood why the k_{eq} value increases with an increase in the tensile load for polymer geosynthetic reinforcements. One possible reason is that slack in the constituting fibres decreases with an increase in the tensile load.
2. At the respective constant load levels, k_{eq} decreases significantly with an increase in the temperature.

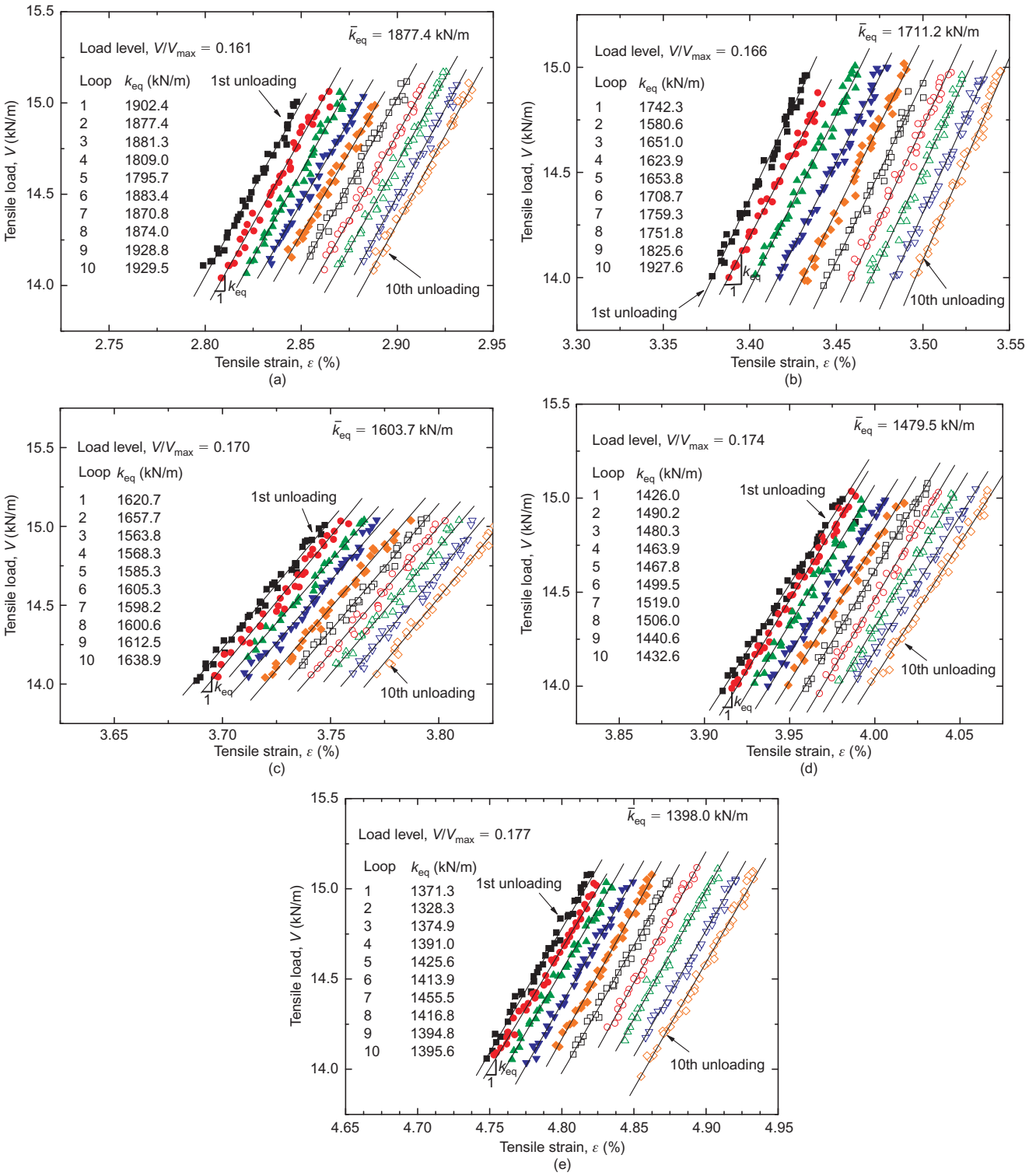

Figure 18. Determination of equivalent elastic stiffness k_{eq} of PP geogrid from unloading branches of small-amplitude unload–reload cycles presented in Figure 17: T = (a) 30°C; (b) 35°C; (c) 40°C; (d) 45°C; (e) 50°C.

Based on the above, the data set of respective geogrid types was fitted by the linear relation

$$k_{eq} = k_{eq0}(T)\left(\frac{V}{V_{max}}\right)^{m} \tag{3}$$

where k_{eq} is the elastic stiffness when the temperature is equal to T and the load level is equal to V/V_{max}; $k_{eq0}(T)$ is the value of k_{eq} when $V = V_{max}$, which decreases with an increase in T; and m is a constant, which is independent of temperature. The values of $k_{eq0}(T)$ and m are different for the different geogrid types. A larger value of m means a larger dependence of k_{eq} on V/V_{max}. The values of k_{eq0} values at different temperatures and the value of m averaged for different temperatures for the various geogrid types are presented in Figures 22a–22c.

The rupture strength corrected to $\dot{\varepsilon} = 0.1\%$/min, V_{max}, at a given temperature can be obtained from the temperature effect parameter $A^{f\prime}$ (Equation 2), which is a function of

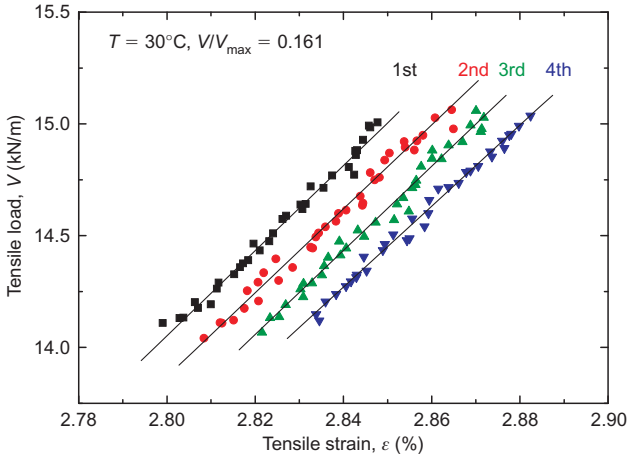

Figure 19. Enlarged relations of those presented in Figure 18a

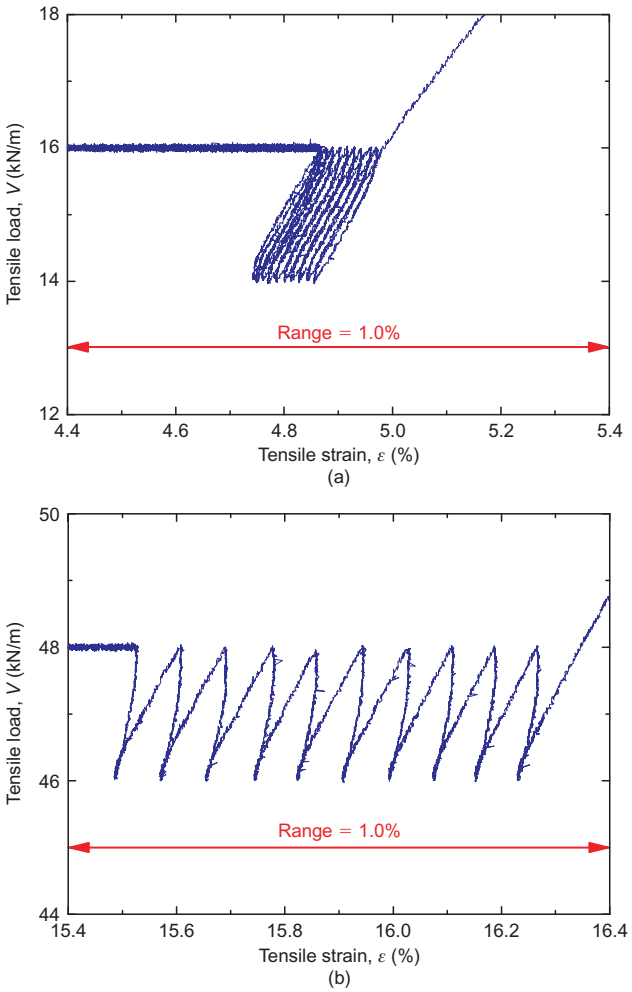

Figure 20. Enlarged V–ε relation of PP geogrid at temperature of 50°C presented in Figure 16a: (a) $V/V_{max} = 0.177$; (b) $V/V_{max} = 0.532$

T, and the rupture strength V'_{max0} at the standard temperature T'_0 (= 20°C). Therefore it is convenient to express $k_{eq0}(T)$ as a function of $A^{f\prime}$, $k_{eq0}(A^{f\prime})$. Figures 23a–23c show the relationships between $k_{eq0}(A^{f\prime})$ and $A^{f\prime}$ for the PP, HDPE and PET geogrids, respectively. Considering that the elastic stiffness should approach zero when the rupture strength approaches zero when the temperature reaches some very high value, the following non-linear equation was assumed, and was fitted to the data for the various geogrid types, as shown in Figures 23a–23c.

$$k_{eq0}(A^{f\prime}) = p(A^{f\prime})^q \tag{4}$$

where p and q are constants. The values of these parameters for the various geogrid types are presented in Figures 23a–23c.

In summary, the elastic stiffness k_{eq} increases with an increase in the load level and decreases with an increase in the temperature (as does the rupture strength). As shown in Figure 24, the value of k_{eq} at a given temperature T and given load V for a given geogrid type can be obtained by substituting Equations 2, 3 and 4: (1) T; (2) V; and (3) the rupture strength at the standard temperature of 20°C when $\dot{\varepsilon} = 0.1\%$/min ($V'_{max0}$). The constants of these equations should be determined specifically for the geogrid type being dealt with. If only the rupture strength at a strain rate other than 0.1%/min is available, this value can be corrected to $\dot{\varepsilon} = 0.1\%$/min by the method described in Section 3.1. The method described in Figure 24 can be easily implemented in the non-linear three-component model (Figure 4). Realistic simulations of the tensile load–strain–temperature behaviour of a given geogrid then become possible, based on this model, and will be reported in the near future by the authors.

4. CONCLUSIONS

The following conclusions can be derived from the experimental results for polypropylene (PP), high-density polyethylene (HDPE) and polyester (PET) geogrids and the analyses presented above.

1. A newly developed automated tensile loading apparatus can control accurately both loading histories and temperature histories.
2. The rupture tensile strength of the tested geogrids decreases with an increase in the temperature, T, from 30°C to 50°C, as tested in this study. This trend was expressed by an empirical function of T, called the temperature effect parameter.
3. The elastic stiffness of the tested geogrids increases with an increase in the tensile load and decreases with an increase in the temperature.
4. Empirical equations to obtain the elastic stiffness at a given temperature and a given tensile load of the three tested geogrid types were developed by incorporating conclusions 2 and 3.

The trends of temperature- and tensile-load-dependent elastic stiffness summarised in conclusions 2 and 3 are similar for the three different types of geogrid tested, as expressed by the empirical equations of same form presented in this study. Further study will be necessary to examine whether the results from the present study can be applied to other types of polymer geosynthetic reinforcement under general temperature and tensile load conditions.

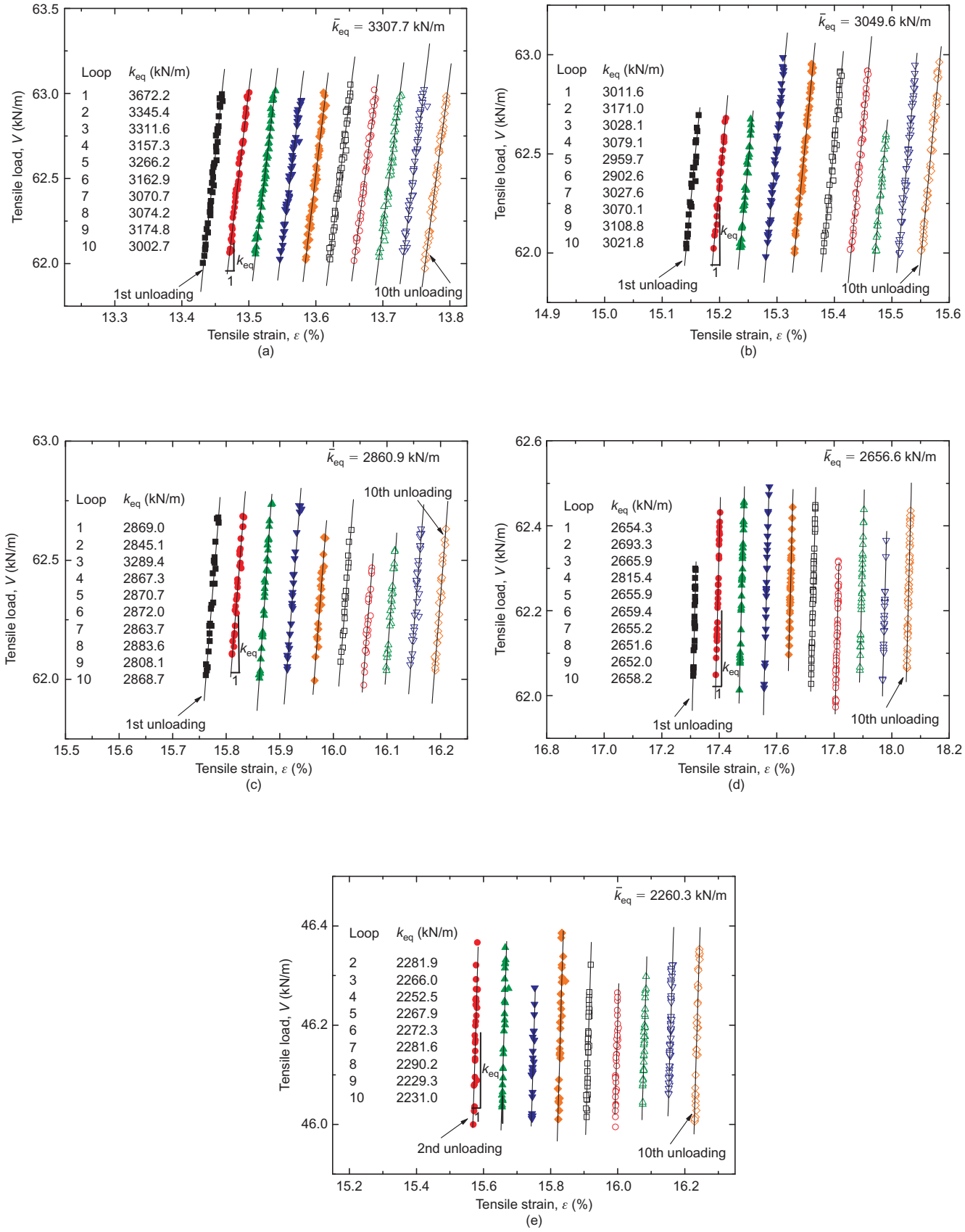

Figure 21. Determination of equivalent elastic stiffness k_{eq} of PP geogrid from unloading branches of small-amplitude unload–reload cycles presented in Figure 16 a at temperature T and load level V/V_{max} of: (a) 30°C and 0.644; (b) 35°C and 0.664; (c) 40°C and 0.682; (d) 45°C and 0.694; (e) 50°C and 0.532

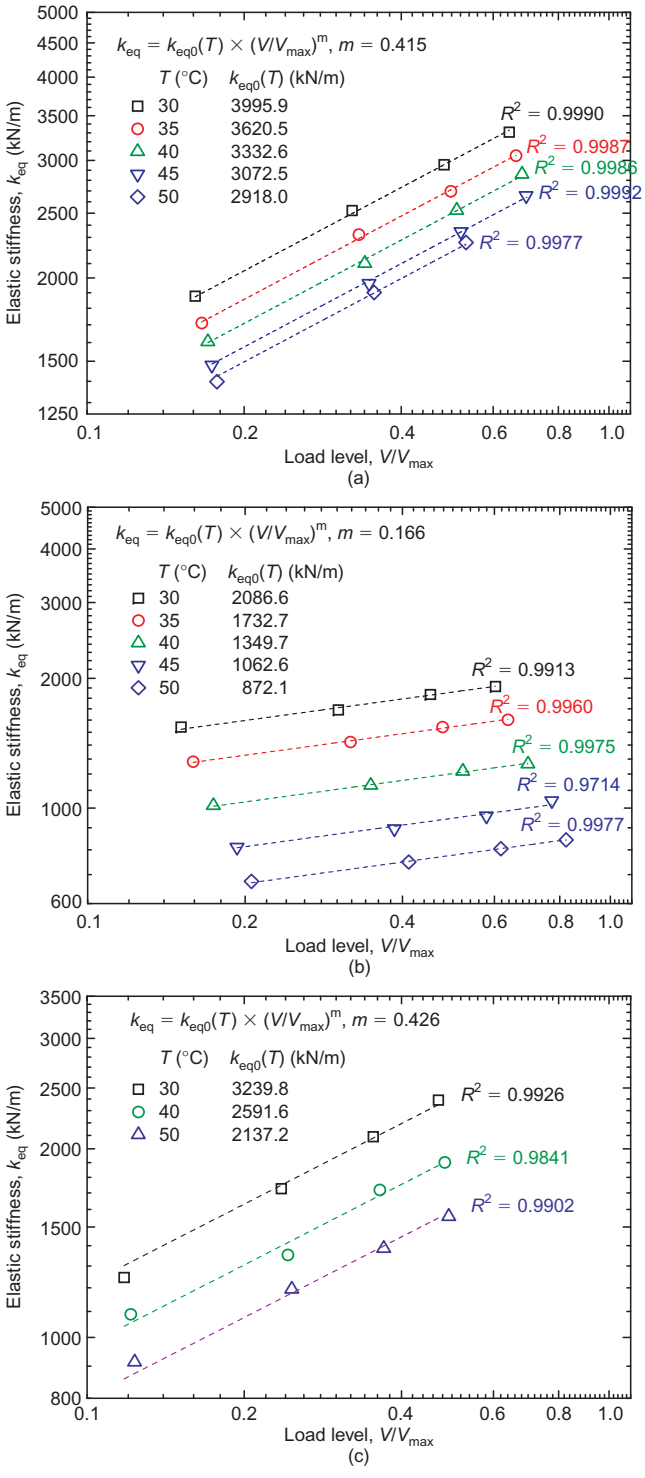

Figure 22. Relationships between equivalent elastic stiffness k_{eq} and load level V/V_{max} at different temperatures obtained for: (a) PP geogrid; (b) HDPE geogrid; (c) PET geogrid

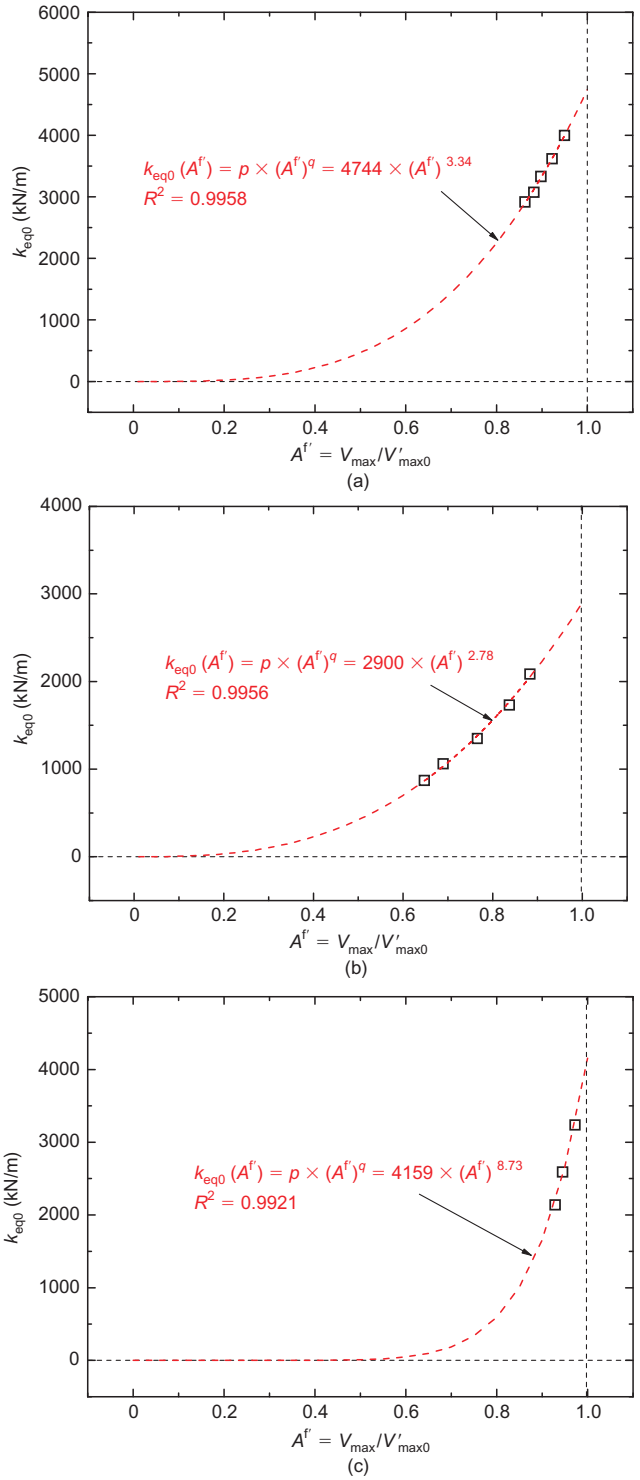

Figure 23. Relationship between k_{eq0} (Equation 3) and temperature effect parameter $A^{f\prime}$ (Equation 2; defined for the standard temperature of 20°C) for respective temperatures obtained from: (a) PP geogrid; (b) HDPE geogrid; (c) PET geogrid

ACKNOWLEDGEMENTS

The authors are grateful to the Commission on Higher Education and the Thailand Research Fund (TRF) for the financial support from Grant No. MRG5280049. Test results from Zornberg *et al.* (2004) in digital format provided by J. G. Zornberg, University of Texas at Austin, are highly appreciated. Advice from P. Jongpradist and S. Youwai is also gratefully acknowledged.

NOTATION

Basic SI units are given in parentheses.

A^f temperature effect parameter defined for reference temperature of 30°C (dimensionless)

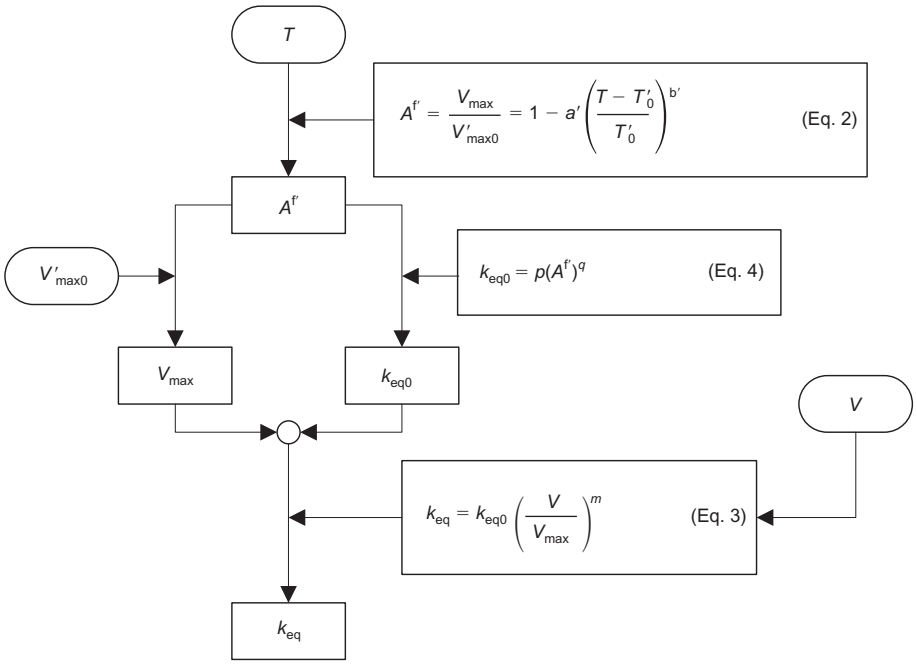

Figure 24. Diagram to obtain elastic stiffness value from current temperature, current tensile load and rupture strength at standard temperature

$A^{f\prime}$ temperature effect parameter defined for standard temperature of 20°C (dimensionless)
a constant of relationship between A^f and temperature (dimensionless)
a' constant of relationship between $A^{f\prime}$ and temperature (dimensionless)
b constant of relationship between A^f and temperature (dimensionless)
b' constant of relationship between $A^{f\prime}$ and temperature (dimensionless)
k_{eq} equivalent elastic stiffness (N/m)
k_{eq0} k_{eq} when tensile load is equal to rupture strength (N/m)
k_{tan} tangent stiffness of tensile load–strain relation (N/m)
m constant of relationship between k_{eq} and load level (dimensionless)
p k_{eq0} when $A^{f\prime} = 1.0$ (N/m)
q constant of relationship between k_{eq0} and $A^{f\prime}$ (dimensionless)
T temperature (°C)
T_0 reference temperature defined at 30°C (°C)
T'_0 standard temperature defined at 20°C (°C)
V tensile load (N/m)
ΔV tensile load jump (N/m)
$\dot{V}$ tensile load rate (N/m s)
V_{max} rupture strength (N/m)
V_{max0} rupture strength at reference temperature defined at 30°C (N/m)
V'_{max0} rupture strength at standard temperature defined at 20°C (N/m)
V^f inviscid tensile load (N/m)
V^v viscous tensile load (N/m)
β rate-sensitivity coefficient (dimensionless)
ε tensile strain (dimensionless)
$\dot{\varepsilon}$ tensile strain rate (s^{-1})
$\dot{\varepsilon}^e$ elastic tensile strain rate (s^{-1})
$\dot{\varepsilon}^{ir}$ irreversible tensile strain rate (s^{-1})
ρ radius of curvature (dimensionless)

ABBREVIATIONS

CL cyclic loading
E/P electropneumatic
HDPE high-density polyethylene
LRFD load and resistance factor design
MD machine direction
ML monotonic loading
PE polyethylene
PET polyester
PP polypropylene
RF reduction factor
RF_{CR} creep reduction factor
RF_D degradation reduction factor
RF_{ID} installation damage reduction factor
SL sustained loading
TD transverse direction

REFERENCES

ASTM D4595. *Standard Test Method for Tensile Properties of Geotextiles by the Wide-Width Strip Method*, ASTM International, West Conshohocken, PA, USA.
ASTM D5262. *Standard Test Method for Evaluating the Unconfined Tension Creep and Creep Rupture Behavior of Geosynthetics*, ASTM International, West Conshohocken, PA, USA.
ASTM D6992. *Standard Test Method for Accelerated Tensile Creep and Creep-Rupture of Geosynthetic Materials Based on Time-Temperature Superposition Using the Stepped Isothermal Method*, ASTM International, West Conshohocken, PA, USA.
Bathurst, R. J., Huang, B. & Allen, T. M. (2011). Interpretation of

installation damage testing for reliability based analysis and LRFD calibration. *Geotextiles and Geomembranes*, **29**, No. 3, 323–334.

Bathurst, R. J., Huang, B.-Q. & Allen, T. M. (2012). Interpretation of laboratory creep testing for reliability-based analysis and load resistance factor design (LFRD) calibration. *Geosynthetics International*, **19**, No. 1, 39–53.

Bueno, B. S., Costanzi, M. A. & Zornberg, J. G. (2005). Conventional and accelerated creep tests on nonwoven needle-punched geotextiles. *Geosynthetics International*, **12**, No. 6, 276–287.

Bush, D. I. (1990). Variation of long-term design strength of geosynthetics in temperatures up to 40°C. *Proceedings of the 4th International Conference on Geotextiles, Geomembranes, and Related Products*, The Hague, pp. 673–676.

Di Benedetto, H., Tatsuoka, F. & Ishihara, M. (2002). Time-dependent shear deformation characteristics of sand and their constitutive modelling. *Soils and Foundations*, **42**, No. 2, 1–22.

EN ISO 10319. *Geosynthetics: Wide-Width Tensile Test*, International Organization for Standardization, Geneva, Switzerland

Ezaoui, A., Tatsuoka, F., Sano, Y., Iguchi, Y., Maeda, Y., Sasaki, Y. & Duttine, A. (2010). Ageing effects on the yielding characteristics of cemented-mixed granular materials. *Soils and Foundations*, **50**, No. 5, 705–724.

FHWA (2001). *Mechanically Stabilized Earth Walls and Reinforced Soil Slopes Design and Construction Guidelines*, Federal Highway Administration (FHWA), NHI Course No. 132042, authored by Elias, V., Christopher, B. R. and Berg, R. R., Washington, DC, USA.

Greenwood, J. H., Kempton, G. T., Brady, K. C. & Watts, G. R. A. (2004). Comparison between stepped isothermal method and long-term creep tests on geosynthetics. *Proceedings of the 3rd European Geosynthetics Conference*, Munich, Vol. 2, pp. 527–532.

GRI (2000). *Standard Test Method for Accelerated Tensile Creep and Creep-Rupture of Geosynthetic Materials Based on Time-Temperature Superposition Using the Stepped Isothermal Method*, Geosynthetic Research Institute, Drexel University.

Hirakawa, D., Kongkitkul, W., Tatsuoka, F. & Uchimura, T. (2003). Time-dependent stress–strain behaviour due to viscous properties of geogrid reinforcement. *Geosynthetics International*, **10**, No. 6, 176–199.

Hoque, E. & Tatsuoka, F. (1998). Anisotropy in elastic deformation of granular materials. *Soils and Foundations*, **38**, No. 1, 163–179.

Hsieh, C., Lee, I. & Tain, Y. (2006). Creep strains of high strength polyester geogrids measured by conventional and accelerated test methods. *Proceedings of the 8th International Conference on Geosynthetics*, Yokohama, Japan, Vol. 4, pp. 1581–1584.

Jones, C. J. F. P. & Clarke, D. (2006). The residual strength of geosynthetic reinforcement subjected to accelerated creep testing and simulated seismic events. *Geotextiles and Geomembranes*, **25**, No. 3, 155–169.

Kongkitkul, W. & Tatsuoka, F. (2007). A theoretical framework to analyse the behaviour of polymer geosynthetic reinforcement in temperature-accelerated creep tests. *Geosynthetics International*, **14**, No. 1, 23–38.

Kongkitkul, W., Hirakawa, D., Tatsuoka, F. & Uchimura, T. (2004). Viscous deformation of geosynthetic reinforcement under cyclic loading conditions and its model simulation. *Geosynthetics International*, **11**, No. 2, 73–99.

Kongkitkul, W., Hirakawa, D. & Tatsuoka, F. (2007a). Viscous behaviour of geogrids; experiment and simulation. *Soils and Foundations*, **47**, No. 2, 265–283.

Kongkitkul, W., Tatsuoka, F. & Hirakawa, D. (2007b). Creep rupture curve for simultaneous creep deformation and degradation of geosynthetic reinforcement. *Geosynthetics International*, **14**, No. 4, 189–200.

Kongkitkul, W., Hirakawa, D. & Tatsuoka, F. (2008). Residual deformation of geosynthetic-reinforced sand in plane strain compression affected by viscous properties of geosynthetic reinforcement. *Soils and Foundations*, **48**, No. 3, 333–352.

Kongkitkul, W., Tabsombut, W., Tatsuoka, F. & Jaturapitakkul, C. (2010a). Effects of ambient temperature on the elastic property of a geogrid. *Proceedings of the International Symposium, Exhibition, and Short Course on Geotechnical and Geosynthetics Engineering: Challenges and Opportunities on Climate Change*, Bangkok, Thailand, 7 –9 December 2010, pp. 381–390.

Kongkitkul, W., Tatsuoka, F., Hirakawa, D., Sugimoto, T., Kawahata, S. & Ito, M. (2010b). Time histories of tensile force in geogrid arranged in two full-scale high walls. *Geosynthetics International*, **17**, No. 1, 12–33.

Koo, H., Kim, D. & Kim, Y. (2006). The stepped isothermal method for lifetime prediction of PET geogrids sheathed in PP. *Proceedings of the 8th International Conference on Geosynthetics*, Yokohama, Japan, Vol. 4, pp. 1555–1558.

Nawir, H., Tatsuoka, F. & Kuwano, R. (2003). Effects of viscous properties on the shear yielding characteristics of sand. *Soils and Foundations*, **43**, No. 6, 33–50.

Shibuya, S., Tatsuoka, F., Teachavorasinskun, S., Kong, X.-J., Abe, F., Kim, Y.-S. & Park, C.-S. (1992). Elastic deformation properties of geomaterials. *Soils and Foundations*, **32**, No. 3, 26–46.

Shinoda, M., Horii, K., Bathurst, R. & Tatsuoka, F. (2002). Investigation of tensile strength after creep and stress relaxation of geogrids. *Proceedings of the 37th Japan National Conference on Geotechnical Engineering*, JGS (Osaka), pp. 773–774 (in Japanese).

Shukla, S. K. & Yin, J.-H. (2006). *Fundamentals of Geosynthetic Engineering*, Taylor & Francis/Balkema, Leiden, the Netherlands, 410 pp.

Tatsuoka, F., Sato, T., Park, C.-S., Kim, Y.-S., Mukabi, J. N. & Kohata, Y. (1994). Measurements of elastic properties of geomaterials in laboratory compression tests. *Geotechnical Testing Journal*, **17**, No. 1, 80–94.

Tatsuoka, F., Hirakawa, D., Shinoda, M., Kongkitkul, W. & Uchimura, T. (2004). Keynote Lecture. An old but new issue: viscous properties of polymer geosynthetic reinforcement and geosynthetic-reinforced soil structures. *Proceedings of the 3rd Asian Regional Conference on Geosynthetics*, Seoul, pp. 29–77.

Thornton, J. S. & Baker, T. L. (2002). Comparison of SIM and conventional methods for determining creep-rupture behavior of a polypropylene geotextile. *Proceedings of the 7th International Conference on Geosynthetics*, Nice, France, Vol. 4, pp. 1545–1550.

Thornton, J. S., Paulson, J. N. & Sandri, D. (1998). Conventional and stepped isothermal methods for characterizing long term creep strength of polyester geogrids. *Proceedings of the 6th International Conference on Geosynthetics*, Atlanta, GA, USA, pp. 691–698.

Zornberg, J. G., Byler, B. R. & Knudsen, J. W. (2004). Creep of geotextiles using time-temperature superposition methods. *Journal of Geotechnical and Geoenvironmental Engineering, ASCE*, **130**, No. 11, 1158–1168.

The Editor welcomes discussion on all papers published in Geosynthetics International. Please email your contribution to discussion@geosynthetics-international.com by 15 October 2012.